Silica Hollow Spheres with Ordered and Radially Oriented Amino-Functionalized Mesochannels

6 AUTHORS, INCLUDING:

Jingui Wang
Nanyang Technological University
36 PUBLICATIONS   **583** CITATIONS

Silica Hollow Spheres with Ordered and Radially Oriented Amino-Functionalized Mesochannels

Jin-Gui Wang, Feng Li, Hui-Jing Zhou, Ping-Chuan Sun, Da-Tong Ding, and
Tie-Hong Chen*

*Institute of New Catalytic Materials Science, Key Laboratory of Energy-Material Chemistry (Tianjin) and
Engineering Research Center of Energy Storage & Conversion (MOE), College of Chemistry, and College
of Physics, Nankai University, Tianjin, 300071, P.R. China*

Using anionic surfactant as templates, ordered mesoporous silica hollow spheres (MSHSs) with radially oriented mesochannels were synthesized with the aid of ultrasonic irradiation. The product was consisted of intact and dispersed hollow spheres with the diameter mostly in the range of 100−500 nm. The hollow spheres possessed uniform shell with the thickness of 35−40 nm, and the shell with radially oriented mesopores exhibited well-ordered structure as confirmed by X-ray diffraction (XRD) and transmission electron microscopy (TEM) measurements. After extraction of the anionic surfactant templates by solvent, silica hollow spheres with ordered and radially oriented amino-functionalized mesochannels were obtained. Moreover, by adjustment of the sonochemical processing time, the shell thickness, mesostructure (hexagonal, radial, or disordered), and shape of the inner cavity (hexagonal or spherical shape) of the hollow spheres could be facilely tuned. The formation process of the radially ordered mesostructure could be attributed to a relatively slow cooperative realignment process of the silica/surfactant hybrid mesophase in this anionic surfactant templating system. The effectiveness of the radially aligned mesopores was validated by a drug (flurbiprofen) release experiment, in which the hollow spheres exhibited relatively high drug storage capacity (>1000 mg g^{-1}) and much faster drug release rate than that of the flakelike mesoporous SBA-15 particles.

Introduction

Mesoporous hollow spheres are appealing candidates in the application fields such as catalysis, biomolecule encapsulation, gene delivery, and controlled drug release. The preparation and modification of hollow spheres with different structures and compositions have attracted great attention. The permeability of the shell influenced by both its thickness and porosity is the key factor for practical applications. It has been reported that well-ordered mesoporous materials with short and accessible channels were favorable for molecular diffusion and mass transfer.[1−4] Up to now, hollow structures with less-ordered mesoporous shell have been synthesized by various methods with the templates of gas bubbles,[5,6] emulsions,[7−9] vesicles,[10−12] and silica (or latex) beads,[13−15] but hollow spheres with ordered mesoporous shell was rarely reported.[16] It would be significant and desirable to fabricate hollow spheres with thin shell-thickness (on the nanometer scale) and orderly oriented mesochannels aligning perpendicular to the shell surface.

Recently, Che and Tatsumi first reported the synthesis of highly ordered anionic surfactant templated mesoporous silica (AMS) materials with anionic surfactant and costructure-directing agent (CSDA) through a new S$^-$N$^+$∼I$^-$ pathway, where S stands for surfactant, N stands for CSDA, and I stands for inorganic precursors.[17] In this pathway, amino-silane (e.g., 3-aminopropyltrimethoxysilane) or quaternized aminosilane (e.g., *N*-trimethoxylsilylpropyl-*N*,*N*,*N*-tributyl-ammonium) were used as CSDA. During the self-assembly process, the positively charged amine or ammonium sites of CSDA interact electrostatically with the templating anionic surfactant micelles and the alkoxysilane sites of CSDA co-condense with the inorganic precursors. This new pathway

---

(1) Deng, Y.; Qi, D.; Deng, C.; Zhang, X.; Zhao, D. *J. Am. Chem. Soc.*
2008, *130,* 28.
(2) Zhang, H.; Sun, J.; Ma, D.; Bao, X.; Klein-Hoffmann, A.; Weinberg,
G.; Su, D.; Schlogl, R. *J. Am. Chem. Soc.* **2004,** *126,* 7440.
(3) Sujandi; Park, S. E.; Han, D. S.; Han, S. C.; Jin, M. J.; Ohsuna, T
Chem. Commun. **2006,** 4131.
(4) Stempniewicz, M.; Khalil, A. S. G.; Rohwerder, M.; Marlow, F. *J. Am.
Chem. Soc.* **2007,** *129,* 10561.
(5) Rana, R. K.; Mastai, Y.; Gedanken, A. *Adv. Mater.* **2002,** *14,* 1414.
(6) Wu, Z.; Zhang, M.; Yu, K.; Zhang, S.; Xie, Y *Chem.−Eur. J.* **2008,**
14, 5346.
(7) Schacht, S.; Huo, Q.; Voigt-Martin, I. G.; Stucky, G. D.; Schüth, F.
Science **1996,** *273,* 768.
(8) Sun, Q. Y.; Kooyman, P. J.; Grossmann, J. G.; Bomans, P. H. H.;
Frederik, P. M.; Magusin, P.; Beelen, T. P. M.; Van Santen, R. A.;
Sommerdijk, N. *Adv. Mater.* **2003,** *15,* 1097.
(9) Botterhuis, N. E.; Sun, Q.; Magusin, P. C. M. M.; van Santen, R. A.;
Sommerdijk, N *Chem.−Eur. J.* **2006,** *12,* 1448.
(10) Kim, S. S.; Zhang, W. Z.; Pinnavaia, T. J *Science* **1998,** *282,* 1302.
(11) Yeh, Y.; Chen, B.; Lin, H.; Tang, C. *Langmuir* **2006,** *22,* 6.
(12) Yu, M. H.; Wang, H. N.; Zhou, X. F.; Yuan, P.; Yu, C. Z. *J. Am.
Chem. Soc.* **2007,** *129,* 14576.
(13) Tan, B.; Rankin, S. E. *Langmuir* **2005,** *21,* 8180.
(14) Arnal, P. M.; Weidenthaler, C.; Schüth, F. *Chem. Mater.* **2006,** *18,*
2733.
(15) Arnal, P. M.; Schüth, F.; Kleitz, F. *Chem. Commun.* **2006,** 1203.
(16) Djojoputro, H.; Zhou, X. F.; Qiao, S. Z.; Wang, L. Z.; Yu, C. Z.; Lu,
G. Q *J. Am. Chem. Soc.* **2006,** *128,* 6320. vesicle.
(17) Che, S.; Garcia-Bennett, A. E.; Yokoi, T.; Sakamoto, K.; Kunieda,
H.; Terasaki, O.; Tatsumi, T. *Nat. Mater.* **2003,** *2,* 801.

Ordered and Radially Oriented Amino-Functionalized MSHSs

Chem. Mater., Vol. 21, No. 4, 2009 613

Scheme 1. Illustration of the Formation of MSHSs and cooperative Realignment Process As Well As the Preparation of Amino-Functionalized Product
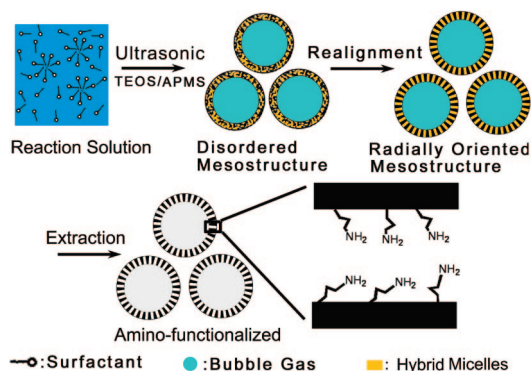
has been proven a successful way to produce a series of novel mesostructured phases, such as lamellar, hexagonal, cubic, and disordered mesostructures,[18-20] as well as well-defined morphologies.[21-27] In addition, mesoporous silica synthesized through the $S^-N^+{\sim}I^-$ pathway would be beneficial to the preparation of surface amino-functionalized mesoporous silica after simple removal of the anionic surfactant by an acid-extraction.[28]

Herein, mesoporous silica hollow spheres (MSHSs) with ordered, radially oriented mesochannels in the shell (35−40 nm in thickness) were first fabricated by using anionic surfactant as the templates. As shown in Scheme 1, the reaction solution (for details, see Experimental Section) was subjected to ultrasonic irradiation. It has been well-accepted that the sonochemical effect is based on acoustic cavitation: the creation, expansion, and implosive collapse of bubbles in ultrasonically irradiated liquid, generating local hot spots of high temperature and pressure.[29-31] In our synthesis system, the bubbles generated by ultrasonic irradiation were stabilized by the surfactant at the gas−liquid interface, and could serve as the template for the hollow structure. During the succedent reaction, the initially formed disordered silica/surfactant hybrid mesophases in the shell underwent a

structural transformation and finally ordered MSHSs with radially oriented mesochannels were obtained. In our synthesis, anionic surfactant was used as the template and the formation of mesophases followed the $S^-N^+{\sim}I^-$ pathway, as described above. Therefore, removal of the anionic surfactant by extraction led to the surface-functionalized sample containing amino groups on the mesopore surface as previous reported.[28] Because mesoporous silica materials have been considered as excellent candidates for controlled drug-delivery systems,[32-34] here the effectiveness of the radially aligned mesopores in the hollow spheres was validated by a drug (flurbiprofen) release experiment.

Experimental Section

Chemicals. *N*-Lauroylsarcosine sodium (Sar-Na) was purchased from Merck, and 3-aminopropyltrimethoxysilane (APMS) was from Acros. All the chemical agents were used without further purification.

Synthesis of Mesoporous Silica Hollow Spheres (MSHS). In a typical synthesis of MSHS, 1.0 mmol of *N*-lauroylsarcosine sodium (Sar-Na) was completely dissolved in 30.0 mL of deionized water under stirring, and 4.0 mL of HCl (0.1 M) was then added to the aqueous solution under vigorous stirring for 1 h at room temperature. Next, 0.10 mL of APMS was added to the above solution and after the solution was stirred for 5 min, 1.5 mL of TEOS was added to the above solution. The final reactant molar ratio is 1890H$_2$O/1.0Sar-Na/0.4HCl/6.7TEOS/0.56APMS. After being stirred for 10 min, the mixture was subjected to an ultrasonic irradiation with a SCINTZ JY92−2D ultrasonic cell crusher for 30−60 s (typically 30 s was used). The cell crusher was operated with a power of 100 W at the frequency of 20−24 kHz, with a pulsed irradiation mode of one-second working and one-second interval. The solution was left at room temperature for 2 h under quiescent condition and then transferred into an 80 °C oven for another 24 h. The white final product was filtrated, washed with deionized water, and dried at 50 °C. To obtain the pure mesoporous silica without the surfactant and aminopropyl moieties, we calcined the as-synthesized samples at 550 °C for 6 h. To prepare the amino-functionalized mesoporous silica (denoted as MSHS-NH$_2$), the surfactant was removed by an acid extraction and the detailed procedure was as followed: 1.0 g as-synthesized sample was stirred in a mixture solution of 100 mL acetonitrile and 10.42 g 36−38 wt % HCl for 24 h at room temperature. The product was filtrated, washed with deionized water and dried at 50 °C.

Drug Loading and Release. Fifty milligrams of mesoporous silica product was added into 2.0 mL of 75 mg mL^{-1} flurbiprofen (FBP) ethanol solution at room temperature. After being dispersed by ultrasound treatment, the mixture was evaporated at 50 °C for 24 h. Next, 2.0 mL ethanol was added to the dried mixture, and the suspension was sealed and left at room temperature for another 2 h. The mesoporous silica adsorbed with FBP (denoted as FBP@SiO$_2$) was separated from the above suspension by centrifugation (at the speed of 8000 rpm for 5 min).

A typical in vitro drug release experiment was performed as follows. The sample of FBP@SiO$_2$ was immersed into 100 mL of phosphate-buffered saline (PBS, 137 mM NaCl, 2.7 mM KCl, 4.3 mM Na$_2$HPO$_4$, and 1.4 mM KH$_2$PO$_4$ in deionized water, pH 7.2−7.4) under stirring at a rate of 100 rpm at room temperature.

(18) Garcia-Bennett, A. E.; Terasaki, O.; Che, S.; Tatsumi, T. *Chem. Mater.* **2004**, *16*, 813.

(19) Garcia-Bennett, A. E.; Miyasaka, K.; Terasaki, O.; Che, S. *Chem. Mater.* **2004**, *16*, 3597.

(20) Gao, C.; Sakamoto, Y.; Sakamoto, K.; Terasaki, O.; Che, S. *Angew. Chem., Int. Ed.* **2006**, *45*, 4295.

(21) Che, S.; Liu, Z.; Ohsuna, T.; Sakamoto, K.; Terasaki, O.; Tatsumi, T. *Nature* **2004**, *429*, 281.

(22) Jin, H.; Liu, Z.; Ohsuna, T.; Terasaki, O.; Inoue, Y.; Sakamoto, K.; Nakanishi, T.; Ariga, K.; Che, S. *Adv. Mater.* **2006**, *18*, 593.

(23) Gao, C.; Qiu, H.; Zeng, W.; Sakamoto, Y.; Terasaki, O.; Sakamoto, K.; Chen, Q.; Che, S. *Chem. Mater.* **2006**, *18*, 3904.

(24) Yu, Y.; Qiu, H.; Wu, X.; Li, H.; Li, Y.; Sakamoto, T.; Inoue, Y.; Sakamoto, K.; Terasaki, O.; Che, S. *Adv. Funct. Mater.* **2008**, *18*, 541.

(25) Wang, J.; Xiao, Q.; Zhou, H.; Sun, P.; Yuan, Z.; Li, B.; Ding, D.; Shi, A.; Chen, T. *Adv. Mater.* **2006**, *18*, 3284.

(26) Wang, J.; Xiao, Q.; Zhou, H.; Sun, P.; Li, B.; Ding, D.; Chen, T. *J. Phys. Chem. C* **2007**, *111*, 16544.

(27) Wang, J.; Xiao, Q.; Zhou, H.; Sun, P.; Ding, D.; Chen, T. *J. Colloid Interface Sci.* **2008**, *323*, 332.

(28) Yokoi, T.; Yoshitake, H.; Yamada, T.; Kubota, Y.; Tatsumi, T. *J. Mater. Chem.* **2006**, *16*, 1125.

(29) Suslick, K. S.; Price, G. *Annu. Rev. Mater. Sci.* **1999**, *29*, 295.

(30) Suslick, K. S. *Science* **1990**, *247*, 1439.

(31) Suslick, K. S.; Choe, S. B.; Cichowlas, A. A.; Grinstaff, M. W. *Nature* **1991**, *353*, 414.

(32) Vallet-Regí, M.; Balas, F.; Arcos, D *Angew. Chem., Int. Ed* **2007**, *46*, 7548.

(33) Slowing, I. I.; Trewyn, B. G.; Giri, S.; Lin, V. S. Y. *Adv. Funct. Mater.* **2007**, *17*, 1225.

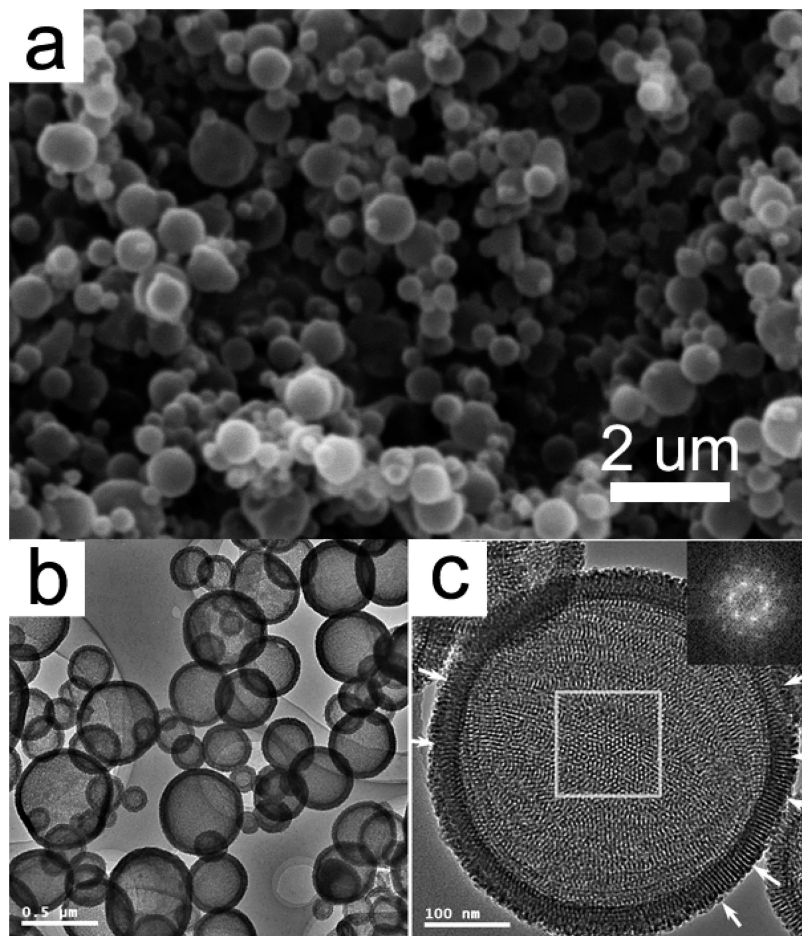(34) Rosenholm, J. M.; Lindén, M. *J. Controlled Release* **2008**, *128*, 157.

Figure 1. (a) SEM and (b, c) TEM images of the ordered MSHSs with radially oriented mesochannels. Inset in (c) is Fourier transform diffractogram of the central area (indicated by rectangle) of the projected TEM image. The white arrows in (c) indicate the direction of the mesochannels.

The release medium (0.2 mL) was removed for analysis at given time intervals, and the same volume of fresh PBS solution was added for compensation. The 0.2 mL of extracted solution was diluted to 10 mL with deionized water and analyzed with UV−vis spectroscopy at a wavelength of 247 nm. By measuring the UV adsorption of several standard FBP solutions, a calibration curve of FBP concentration versus UV adsorption was set up as $A = 0.0808C + 0.0152$, where A is the absorbance and C is the FBP concentration (μg mL^{-1}). The release amount of the FBP was then calculated by this calibration curve. The total FBP amount of release for 6 days was determined as the total storage of the mesoporous silica. TG/DTA measurements were used to determine the amount of left FBP in the mesoporous silica after 6 days of FBP release and the results indicated that almost all FBP loaded on the silica was released in the PBS solution.

Characterization. TEM observations were performed on a Philips Tecnai F20 microscope, working at 200 kV. All samples subjected to TEM measurements were dispersed in methanol ultrasonically and were dropped on copper grids. SEM images were obtained with a Shimadzu SS-550 instrument. X-ray diffraction (XRD) pattern was obtained on a Rigaku D/max-2500 diffractometer, with Cu Kα radiation at 40 kV and 100 mA. Small-angle X-ray scattering (SAXS) experiments were performed on a Bruker Nanostar small-angle X-ray scattering system. Nitrogen adsorption and desorption isotherms were measured on a BELSORP-mini II sorption analyzer at 77 K. Specific surface area was calculated by BET (Brunauer−Emmett−Teller) method, the pore-size distribution was calculated from the adsorption branch using BJH (Barett−Joyner−Halenda), and total pore volume was obtained at P/P_0 about

0.9. TGA was performed in air with a Rigaku thermogravimetry-differential thermal analysis (TG/DTA) analyzer. ^{29}Si MAS NMR spectra were recorded on a Varian Infinity plus 400 instrument with a π/4 pulse, 20 s recycle delay, and 4 kHz spin rate. ^{13}C CPMAS NMR spectra were measured with a spin rate of 12 kHz, 0.8 ms contact time, and 3 s recycle delay. The Fourier transform infrared (FTIR) transmission spectra spectroscopy were recorded using Bruker VECTOR 22 spectrometers with wavenumber precision <0.01 cm^{-1} and signal-to-noise 30000:1. The elemental analysis was performed on an Elementar Vario-EL instrument. The UV−vis absorbance was measured on a 752N spectroscope of Shanghai Precision & Scientific Instrument Co., Ltd.

Results and Discussion

SEM image (Figure 1a) displays that the obtained as-prepared sample was consisted of dispersed spheres. TEM images (images b and c in Figure 1) show that all the particles were hollow spheres, which were intact without aggregation. By measuring the diameter of the particles from the TEM images, it was found that the particle size was mostly in the range of 100−500 nm (see Figure S1 in the Supporting Information). The particles could be dispersed well in water to form stable suspension for several days (see Figure S2 in the Supporting Information). It is interesting that all the hollow spheres possess uniform shell thickness of 35−40 nm, independent of their sizes. The significant feature of the hollow spheres was the radially oriented mesochannels in
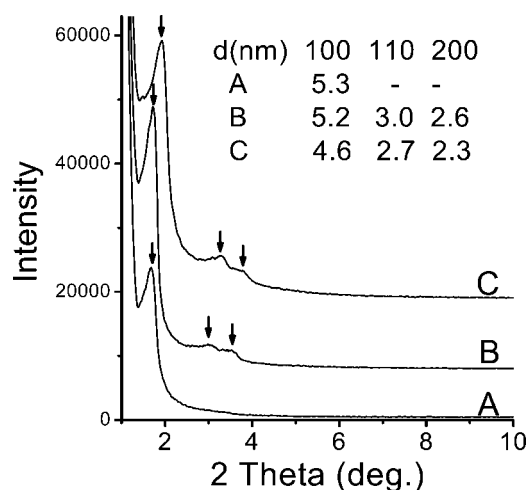
Figure 2. XRD patterns of (A) the as-synthesized (synthesized with 30 s of ultrasonic treatment and 24 h at 80 °C), (B) solvent extracted, and (C) calcined MSHSs with radially oriented mesochannels.

their shells. It can be clearly observed that the mesochannels aligned along the normal direction of the shell surface and perforated the shell (Figure 1c). In the central area of the hollow spheres, clearly observable spot-pores also confirm that the mesochannels ran through from the spherical surface to the interior. Moreover, Fourier transform diffractogram (inset of Figure 1c) of the central area of the TEM image indicates ordered hexagonal packing of the mesopores.

The TEM image (see Figure S3 in the Supporting Information) shows that the hollow morphology was well retained after calcination at 550 °C for 6 h. It is reasonable that the as-synthesized MSHS exhibited only one peak in its XRD pattern (Figure 2a) because of the presence of the surfactant templates which decreased the contrast of the diffraction. XRD patterns (patterns b and c in Figure 2) indicate that both the solvent-extracted (amino-functionalized mesoporous silica) and the calcined (pure silica mesoporous material) MSHSs possessed 2D hexagonal structures as determined by the three distinct diffraction peaks, though on the spherical shell the packing of the radially oriented mesopores could be distorted from a perfect 2D hexagonal structure to a certain extent. The N_2 adsorption–desorption isotherms of both the solvent-extracted and calcined MSHSs show type IV isotherm with an adsorption step at partial pressure between 0.3–0.5 due to the capillary condensation of the filling nitrogen in the mesopores (Figure 3). The pore size distribution was very narrow with a peak centered at 3.0 nm for the solvent-extracted sample and 3.1 nm for the calcined sample respectively, indicating the uniform sizes of the mesopores. The BET specific surface areas of the solvent-extracted and calcined MSHSs were 427 and 502 $m^2\ g^{-1}$, and the pore volumes were 0.44 and 0.50 $cm^3\ g^{-1}$, respectively. Both the samples exhibited hysteresis loops at higher partial pressures of about 0.5, which had also been observed for other hollow structures with mesoporous walls,[10,13,35−37] and probably were due to the delay of nitrogen evaporation from the hollow voids blocked by the surrounding mesopores during the N_2 desorption process.[38] For the solvent-extracted sample, because of the presence of the surface functionalized amino groups in the mesochannels,

the pore size was slightly smaller than that of the calcined samples, which would result in different pore blocking effect to the nitrogen evaporation from the hollow space and thus gave rise to a slightly different hysteresis loop in the desorption isotherm (Figure 3a), if compared with that in the desorption isotherm of the calcined sample (Figure 3c).

If the ultrasonic irradiation was not applied in the synthesis, only solid mesoporous silica particles were obtained (Figure 4). This indicates that formation of the hollow particles should be ascribed to the ultrasonic irradiation and the gas bubbles generated by the ultrasonic cavitation acted as the template for the hollow particles.[5,29−31] The orderly aligned mesopores perpendicular to the surface of the shell was an interesting feature and time-dependent syntheses were performed to monitor the mesostructure evolution of the ordered MSHSs. The sample collected after ultrasonic treatment but without heating reaction (denoted as 0 h sample) exhibited already hollow structure. The TEM image displays the randomly arranged mesopores in the shell (Figure 5a) and the SAXS pattern shows only one peak (Figure 6a), indicating that at this stage the mesophase in the shell was lack of long-range order. After ultrasonic treatment and 1 h of reaction at 80 °C, the order of mesophase increased as observed by TEM (Figure 5b). The SAXS pattern shows two peaks, which could be indexed to (100) and (110) diffraction according to the *P6mm* symmetry structure (Figure 6b). However, the obtained spheres were still aggregated and were easily broken (see Figure S4 in the Supporting Information). The sample after 4 h aging at 80 °C exhibited higher order of mesostructure in the shell than that of the 1 h 80 °C aging sample (Figure 5c), and the SAXS pattern displays already three peaks (Figure 6c). However, the hollow spheres were still less robust than the final product of 24 h aging and were easily broken during the filtering and drying preparation (see Figure S4 in the Supporting Information). After 24 h of reaction at 80 °C, ordered mesoporous silica hollow spheres were fabricated with intact and dispersed appearance as described above. Therefore, it is confirmed that the mesophase in the shell of the hollow spheres gradually adjusted to increase its long-range order with the reaction time. ^{29}Si MAS NMR spectra of the as-synthesized samples obtained at 80 °C for 1 and 24 h, respectively, were shown in Figure 7. The less proportion of Q^3 and Q^2 ($Q^n = Si(OSi)_n(OH)_{4−n}$) indicates higher degree of silica condensation for the sample synthesized at 80 °C for 24 h. It must be noted that for the samples collected after 0, 1, and 4 h aging at 80 °C, the coassembly between the surfactants and silica precursors was still unfinished. The interruption of the coassembly process and the following cooling, filtering and drying treatment would result in deformation of the silica hollow spheres and nonuniform thickness of the shell as shown in Figure 5. Moreover, shorter reaction time at 80 °C resulted in lower crosslinking degree and less amount (thinner layer) of the

(35) Lind, A.; Spliethoff, B.; Lindén, M. *Chem. Mater.* **2003**, *15*, 813.
(36) Karkamkar, A. J.; Kim, S.; Mahanti, S. D.; Pinnavaia, T. J. *Adv. Funct. Mater.* **2004**, *14*, 507.
(37) Lin, H. P.; Wong, S. T.; Mou, C. Y.; Tang, C. Y. *J. Phys. Chem. B* **2000**, *104*, 8967.
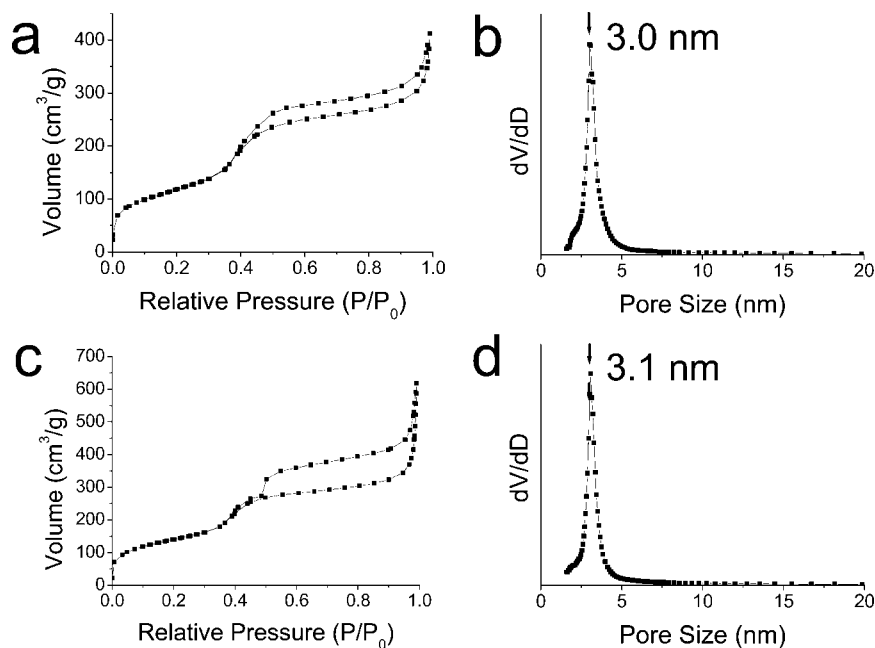(38) Tan, B.; Lehmler, H. J.; Vyas, S. M.; Knuston, B. L.; Rankin, S. E. *Adv. Mater.* **2005**, *17*, 2368.

Figure 3. Nitrogen adsorption−desorption isotherms and the pore size distribution of the (a, b) solvent-extracted and (c, d) calcined MSHSs.
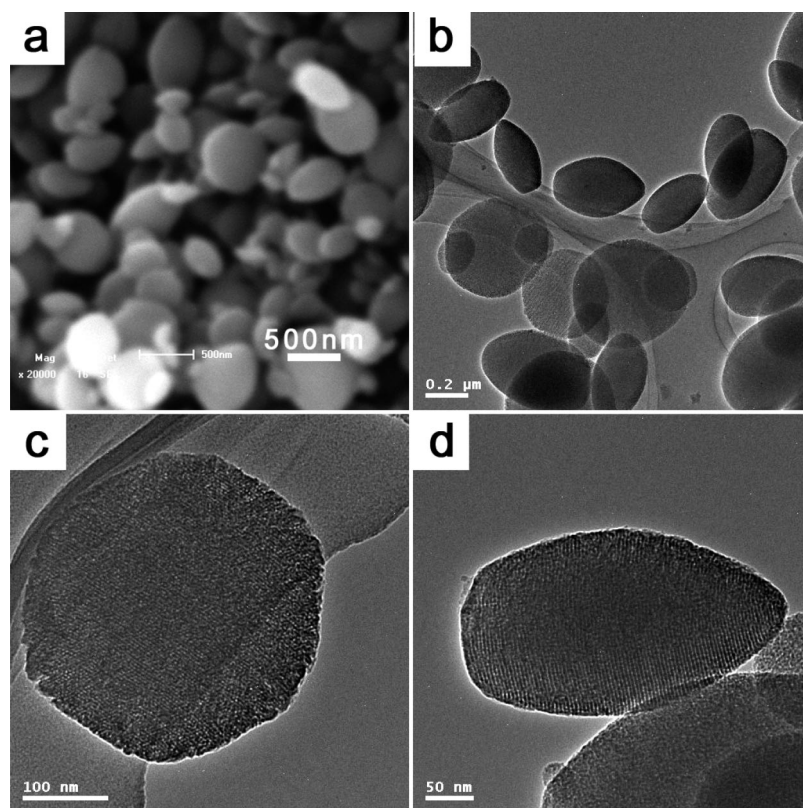

Figure 4. (a) SEM image and (b−d) TEM images of the sample obtained without ultrasonic irradiation.

silica condensed around the surfactant micelles, and thus the samples collected after shorter reaction time contained relatively higher weight percent of the surfactants (Table 1). During the calcination at 550 °C, the thinner layer of the less crosslinked silica on the surfactant micelles underwent further condensation and shrinkage to a greater extent, and this would lead to decreased pore sizes for the samples collected after shorter reaction time at 80 °C (Table 1).

The higher crosslinking degree of the silica and the narrower pore size distribution (Figure 6b) after longer reaction time indicate that there was a cooperative realignment process of the mesophase in the shell to achieve finally the ordered mesostructure. It should be noted that the formation mechanism of the radially ordered mesoporous structure resembles that as was reported by Tan et al., who proposed that the CTAB/silica aggregates deposited as a
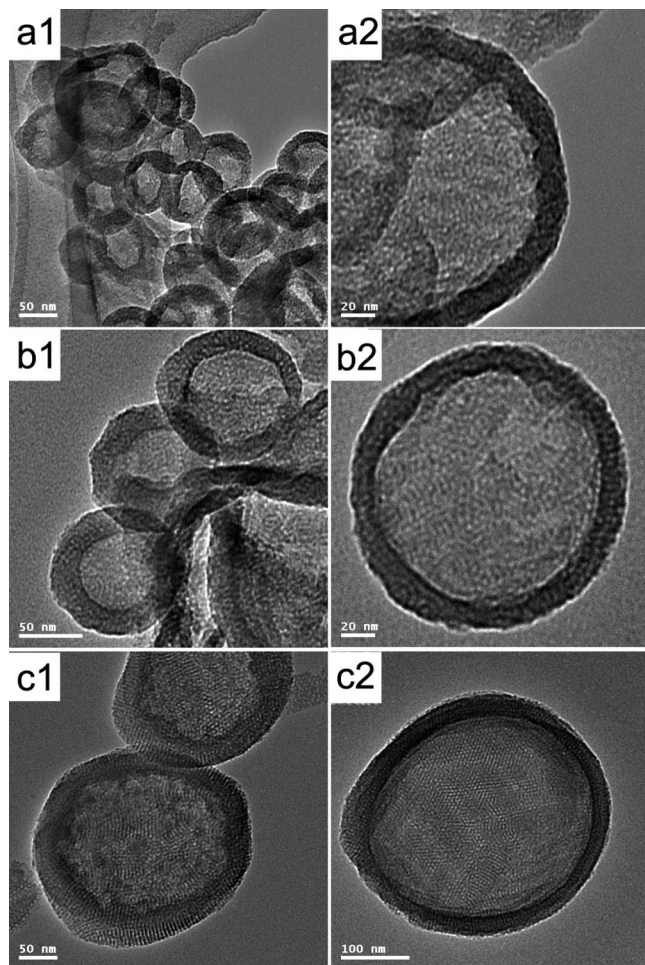
Figure 5. TEM images of the samples synthesized at 80 °C for (a1, a2) 0 (only ultrasonic without heating treatment), (b1, b2) 1, and (c1, c2) 4 h, respectively.

Figure 6. (a) SAXS patterns and (b) pore size distributions of the calcined samples synthesized at 80 °C for 0, 1, and 4 h, respectively.
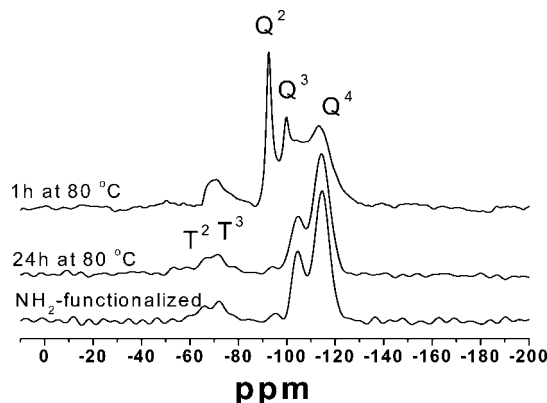
Figure 7. ^{29}Si MAS NMR of the as-synthesized samples obtained at 80 °C for 1 and 24 h, as well as the amino-functionalized sample after surfactant-extraction, respectively, in which $Q^n = Si(OSi)_n(OH)_{4-n}$, $T^n = R$-$Si(OSi)_n(OH)_{3-n}$.

disordered liquidlike phase and then evolved to hexagonally packed mesostructure.[13,39] However, in our synthesis systems using anionic surfactant as the templates, the mesophase transformation in the shell experienced a relatively long time (longer than 60 min), which was different from the fast formation of the ordered structure in the cationic surfactant templating system (within several minutes).[39,40] This relatively slow liquid crystal phase evolution would be favorable for the mesophase assembly to form novel and stable ordered mesostructures after the formation of a specific morphology.

The shell thickness and mesostructure could be facilely tuned by controlling the sonochemical processing time because longer ultrasonic irradiation time would generate more gas bubbles available as templates for production of the hollow morphology. When there were more gas bubbles acting as templates, the silica/surfactant hybrid available to encapsulate each gas bubble would decrease, leading to the reduction of the shell thickness. In contrast, the shell thickness would increase when the ultrasonic irradiation time was shortened. TEM images show that the sample after 12 s of ultrasonic irradiation possessed thicker shell (50−60 nm)
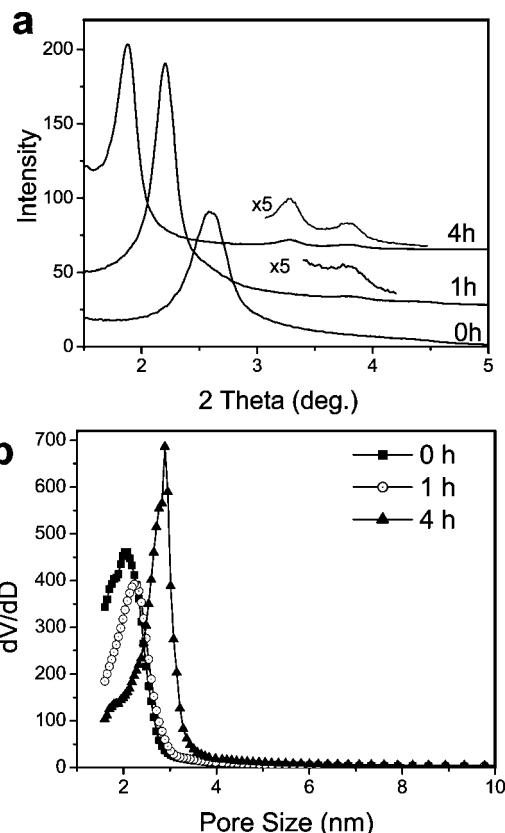
(39) Tan, B.; Rankin, S. E. *J. Phys. Chem. B* **2004**, *108*, 20122.
(40) Sadasivan, S.; Fowler, C. E.; Khushalani, D.; Mann, S. *Angew. Chem., Int. Ed.* **2002**, *41*, 2151.

and hexagonal inner cavities (images a and b in Figure 8). The XRD pattern (Figure 9a) reveals the highly ordered *P6mm* structure, indicating that the higher amount of silica/surfactant hybrid (thicker shell) was beneficial to the formation of a higher ordered structure in the cooperative realignment process of the mesophase. As mentioned above, the sample subjected to 30 s of ultrasonic irradiation exhibited uniform shell thickness of 35−40 nm with the ordered radially oriented mesochannels. The product of 60 s ultrasonic irradiation shows the similar radial-pore structure to that of the 30 s ultrasonic treatment sample (images c and d Figure 8), but the order of the mesophase slightly

Table 1. Structural Parameters of the Calcined Samples Synthesized at 80 °C for 0, 1, 4, and 24 h

time (h)	surface area (m^2/g)	pore size (nm)	pore volume (cm^3/g)	d_{100} $(nm)^a$	weight loss $(wt \%)^b$
0^c	1083	2.0	0.59	3.4	46
1	799	2.3	0.50	4.0	38
4	772	2.9	0.60	4.6	33
24	502	3.1	0.50	4.8^d	22

^{a} All the values were measured by SAXS (Bruker Nanostar system). ^{b} The weight loss of surfactants was estimated by the weight loss between 150 and 550 °C. ^{c} 0 h means that the sample was prepared as the method described in the Experimental Section, after 30 s of ultrasonic treatment but without further heating treatment in the 80 °C oven. ^{d} This value was slightly different from the value measured by XRD (Rigaku D/max-2500 diffractometer), which was 4.6 nm.
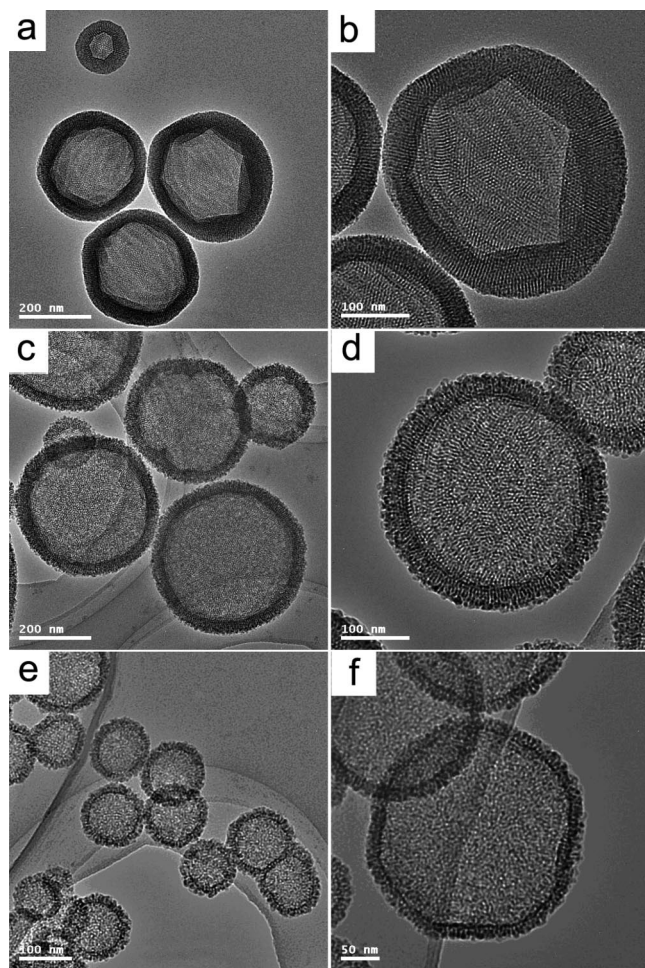
Figure 8. TEM images of the MSHSs synthesized with ultrasonic irradiation for (a, b) 12, (c, d) 60, and (e, f) 180 s, respectively.

Figure 9. XRD pattern of the calcined MSHSs synthesized with ultrasonic irradiation for (a) 12, (b) 60, and (c) 180 s.

Table 2. Structural Parameters of the Calcined Samples Synthesized with Ultrasonic Irradiation Time of 12, 30, 60, and 180 s

time of ultrasonic irradiation (s)	surface area (m^2/g)	pore size (nm)	pore volume (cm^3/g)	shell thickness (nm)	d_{100} $(nm)^a$
12	629	3.0	0.58	50−60	4.6
30	502	3.1	0.50	35−40	4.6
60	538	3.2	0.59	35−40	4.5
180	433	3.2	0.52	15−20	not detected

^{a} All the values were measured by XRD (Rigaku D/max-2500 diffractometer).
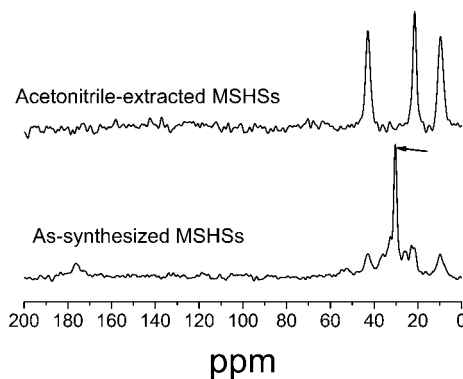
Figure 10. ^{13}C CP/MAS NMR spectrum of as-synthesized MSHSs and acetonitrile-extracted MSHSs. The arrow indicates the ^{13}C signal from the alkyl chain of the surfactant.

decreased as shown in its XRD pattern (Figure 9b). When the ultrasonic irradiation time was prolonged to 180 s, a thinner shell (15−20 nm) was formed and the shell was of disordered mesostructure as shown in the TEM images (images e and f in Figure 8) and XRD pattern (Figure 9c). All the porosity parameters and the mesostructures of the samples subjected to ultrasonic treatment for different times are summarized in Table 2. Moreover, further increasing the ultrasonic irradiation time, the thickness, and the disordered mesostructure of the shell did not change obviously. However, if the ultrasonic irradiation time was shorter than 12 s, solid particles appeared in the product.

Importantly, because our samples were synthesized through the $S^-N^+ \sim I^-$ route and as reported previously,[28] surface amino-functionalized products could be obtained after extraction of the surfactants with a mixture of acetonitrile and HCl at room temperature. The solvent-extracted sample was subjected to various characterizations to further confirm the complete removal of surfactant and the reservation of the amino-groups. ^{13}C CP/MAS NMR spectrum (Figure 10) of the as-synthesized MSHSs shows a strong resonance signal centered at about 30 ppm (indicated by the arrow) and a weak peak at about 176 ppm, which were attributed to the alkyl chain and the carbonyl of the *N*-lauroylsarcosine surfactant, respectively. These signals disappeared in the ^{13}C CP/MAS NMR spectrum of the acetonitrile-extracted sample, demonstrating that the surfactant molecules had been completely removed. In addition, the resonance signals at 9.7,

Ordered and Radially Oriented Amino-Functionalized MSHSs

Chem. Mater., Vol. 21, No. 4, 2009 619

21.5, and 42.9 ppm were assigned to the carbons of the aminopropyl group in APMS, in consistent with the literature.[23] Moreover, FT-IR spectra (see Figure S5 in the Supporting Information) shows that the peaks at 2925 and 2854 cm^{-1} corresponding to the C−H vibrations of the surfactant molecules in the mesopores greatly decrease in the acetonitrile-extracted sample, which also indicates the efficient removal of the surfactant. TG measurement (see Figure S6 in the Supporting Information) shows that the weight loss was 22% for the as-synthesized sample and 4% for acetonitrile-extracted sample in the range of 150−550 °C, confirming again the removal of the surfactant. The remaining amino groups in the sample were also confirmed by the ^{29}Si MAS NMR spectrum (Figure 7) because of the presence of the resonance signals of T^2 and T^3 silicons (T^n = R-Si(OSi)$_n$(OH)$_{3-n}$) originating from APMS used in the synthesis. It is worth noting that most of the amino groups would reside on the surface of the mesochannels because the formation of the mesostructured silica follows the S$^-$N$^+$∼I$^-$ pathway in our synthesis. All these results clearly indicate that after surfactant extraction, the surface amino-functionalized MSHSs were obtained. Elemental analysis result shows that the amount of the organic group of −(CH$_2$)$_3$NH$_2$ in the sample was 1.2 mmol g^{-1}. Therefore, the surface density of the amino groups was about 1.7 amino moieties nm^{-2}, as calculated from the elemental analysis and the BET surface area of 427 m^2 g^{-1}. The solution stability of the amino-functionalized mesoporous hollow spheres in saline solution was checked. The sample was soaked in PBS solution for 8 days and the quantity of the −(CH$_2$)$_3$NH$_2$ groups remained unchanged (checked by EA), indicating that there was no leaching of the surface amino groups in the saline solution.

The average size of the hollow spheres was about 200 nm (Figure S1). It has been shown that nonphagocytic eukaryotic cells could internalize particles as large as 500 nm in size and the uptake efficiency was high for particles around 200 nm or smaller,[41] so the hollow spheres would be potentially useful in drug delivery applications. The drug of FBP was used to examine the storage capacity and release behavior of the hollow spheres with the radially oriented mesochannels. For comparison, mesoporous silica SBA-15 with the flake-like morphology and thickness of about 400 nm (see Figure S7 in the Supporting Information) was also used for drug storage and release tests. Both the amino-functionalized and pure silica hollow samples with radially oriented mesopores exhibited high storage capacity (>1000 mg g^{-1}) and high rate of release (less than 5 h to reach its approximate maximal release amount) (Figure 11 and Table S1 in the Supporting Information), indicating the large cavity of the hollow structure and the favorable molecular diffusion through the radially oriented mesopores. In addition, the release rate of pure silica hollow sample obtained after calcination is only slightly faster than that of the amino-functionalized sample, as shown in Figure 11a. The reason could be attributed to the presence of the amino groups on the surface of the mesoporous channels. However, though
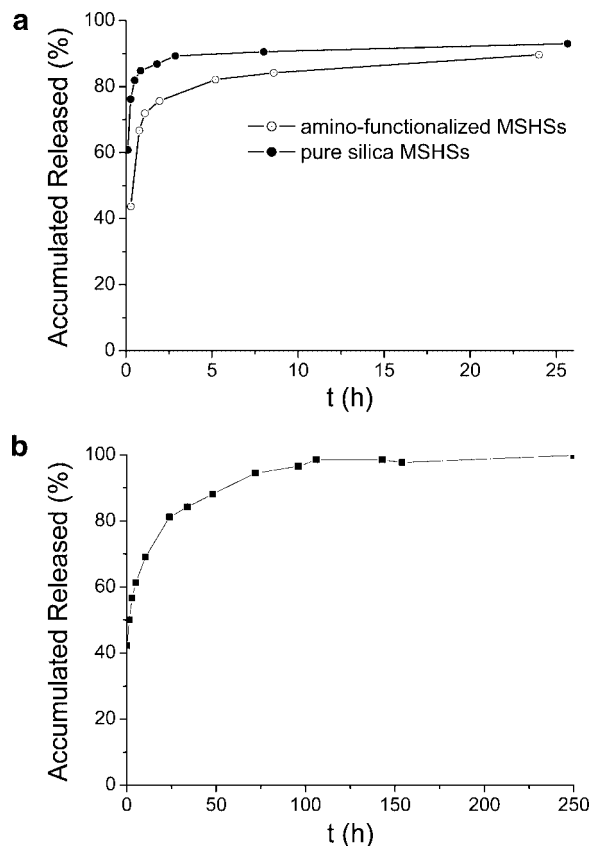

Figure 11. FBP release behavior of (a) the amino-functionalized and calcined pure silica MSHSs and (b) flakelike SBA-15 mesoporous silica.

the amino groups on the surface of the mesoporous channels could interact with the carboxyls of the FBP molecules, the remaining silanols on the silica surface could also influence the drug−support interactions,[34] and thus the release rate of the FBP from the amino-functionalized sample was not much different from that of the calcined sample. In contrast, although the pore size of mesoporous silica SBA-15 discs (8.6 nm) is much larger than that of the mesoporous silica MSHSs (3.0−3.1 nm), SBA-15 exhibited a much slower rate of release (more than 4 days to reach its approximate maximal release amount). The lower release rate would be ascribed to the longer mesoporous channels of 400 nm (see Figure S7 in the Supporting Information), which was much longer than the length of the channels in the shell of MSHSs (35−40 nm). Therefore, the short and easily accessible channels of MSHSs are essential for molecule diffusion. In addition, the FBP drug loading amount of SBA-15 was lower than that of the MSHSs despite the total pore volume of SBA-15 was lager than that of the hollow silica (see Table S1 in the Supporting Information), and this indicates the cavity of the hollow structure could be filled by the FBP drug and thus the drug loading amount was efficiently increased. Generally sustained release of drugs was superior to relatively fast release; however, the MSHSs with radially oriented mesopores would be advantageous to stimulated concentrative release of drugs if modified with proper polyelectrolyte as stimuli-responsive outer layer.[42]

(41) Rejman, J.; Oberle, V.; Zuhorn, I. S.; Hoekstra, D *Biochem. J.* **2004**, *377*, 159.

(42) Zhu, Y. F.; Shi, J. L.; Shen, W. H.; Dong, X. P.; Feng, J. W.; Ruan, M. L.; Li, Y. S. *Angew. Chem., Int. Ed.* **2005**, *44*, 5083.

Conclusion

Intact and stable silica hollow spheres with ordered radially oriented mesochannels and uniform thin shells were successfully synthesized using anionic surfactant as templates. After extraction of the anionic surfactant templates, silica hollow spheres with ordered and radially oriented amino-functionalized mesochannels were obtained. Moreover, the shell thickness, mesostructure (hexagonal, radial, or disordered), and shape of the inner cavity (hexagonal or spherical shape) of the hollow spheres could be facilely tuned. The formation process of the radially ordered mesostructure could be ascribed to a relatively longer cooperative realignment process of the mesophase in the anionic surfactant templating system. The effectiveness of radially aligned mesopores was validated by a drug release experiment with flurbiprofen and the hollow spheres exhibit higher storage capacity ($>$1000 mg g^{-1}) and much higher rate of release compared with flake-like mesoporous SBA-15 particles. The hollow spheres with large cavity and short mesochannels would have potential applications on catalysis, biomolecular encapsulation, and targeted stimulative release of drugs.

Supporting Information Available: Particle size distribution, photo of the suspended MSHSs in the DI water, TEM images, SEM images, FT-IR spectra, and TG curves of the samples (PDF). This material is available free of charge via the Internet at http://pubs.acs.org.

CM803124A